Linear polarization state encoding for Ising computing with optically injection-locked VCSELs

Brandon Loke,[a] **Zifeng Yuan**[iD]**,**[a] **Soon Thor Lim,**[b] **and Aaron Danner**[iD][a,*]
[a]National University of Singapore, Department of Electrical and Computer Engineering, Singapore
[b]Institute of High Performance Computing, Singapore

ABSTRACT. Vertical cavity surface-emitting (VCSEL) arrays offer an attractive platform to develop a photonic Ising computer due to their scalability and compact physical size. Ising interactions can be encoded between VCSELs through mutual optical injection locking, with the polarity of the interaction determined by the presence or absence of a half-wave plate in the optical path, and the bit itself represented by polarization state. The performance of this approach is investigated computationally by extending the spin-flip model to describe a system of mutually injection locked VCSELs for 2-, 3-, and 4-bit Ising problems. Numerical simulations demonstrate that the modeled system solves the given Ising problems significantly better than chance, with critical parameters in the model identified as crucial for achieving an unbiased Ising solver. The quantum well gain anisotropy parameter as well as the ratio of phase anisotropy to decay rate of the local carrier number causes the system to favor particular Ising configurations over others, but this may not prohibit the system from reaching the ground state.

1 Introduction

Many important computational problems lie in difficult-to-solve complexity classes and often require an optimal solution out of many possible options. These combinatorial optimization problems are solved poorly by von Neumann computing architectures, which are bottlenecked by the separation of the instruction set and data operation. In contrast to this, Ising model computing is a non-conventional type of computing that shows great potential for tackling these problems.[1] This form of computing is non-von Neumann, allowing for high parallelization, thereby circumventing some of the bottlenecks present in conventional computing architectures. The Ising model traditionally describes magnetism in materials, where magnetic moments in the model can have a spin-up or spin-down orientation, represented by the states $|+1\rangle$ and $|-1\rangle$, respectively. The Hamiltonian for the Ising system, H, is described through

$$H = \sum_{i<j}^{M} J_{ij}\sigma_i\sigma_j + \sum_{i=1}^{M} h_i\sigma_i, \qquad (1)$$

where σ_i and σ_j are the spin states of the i'th and j'th spin sites, respectively. J_{ij} denotes the coupling strength between the two spin states i and j, whereas h_i is the Zeeman term representing

*Address all correspondence to Aaron Danner, adanner@nus.edu.sg

the interaction the spin at site i experiences due to an external field. As with many physical systems, materials described by the Ising model will tend toward the lowest energy state configurations through thermal spin flips until the Hamiltonian is minimized.

The use of photonic systems to solve Ising problems has been the recent focus of intense research. Photonic Ising machines include spatially multiplexed and fully optical,[1–5] spatially multiplexed and optoelectronic,[6–9] time-multiplexed and fully optical,[10] time multiplexed and optoelectronic,[11–13] among others. Ising states can be encoded into the phase,[2–4,8,12,14] the intensity,[15] or the polarization.[1] Schemes proposed in recent studies often feature an optical parametric oscillator in an optoelectronic feedback configuration[12,14] or a spatial light modulator to perform mathematical operations optically.[3,7–9,16–18]

The Ising model can also be mapped onto a laser-based system through injection locking,[1] whereby light from one laser is directed into the cavity of another laser. This Ising solver is not as well-developed as the other methods, with the only known instances of this being achieved so far by encoding Ising spins onto the phase of light in a fiber laser[2] and the phase of light in two semiconductor lasers.[2]

Vertical cavity surface-emitting lasers (VCSELs) are suitable candidates for such an Ising computer due to their scalability, small physical size, and high Q-factor, which makes injection injection-locking VCSELs easier to achieve than in edge emitting lasers.[19] In addition to this, VCSELs tend to naturally be linearly polarized in one of two orthogonal directions, termed herein as the x- and y-polarizations.[20] A VCSEL with a hypothetically symmetric gain and a cylindrical cavity would lase at any angle between x and y with equal probability. However, the aperture of the VCSEL can be engineered so that either x- or y-polarizations, but not both simultaneously, is preferred.[21] Furthermore, crystal birefringence can cause a preference for x- or y-polarized modes through quantum well gain anisotropy.[20] The inclusion of external injection locking providing additional feedback assists the laser arriving in a single linear polarization state, as has been shown in the experimental results.[22,23] For this reason, the linear polarization directions in a VCSEL are excellent candidates for encoding Ising states. Using this feature of VCSELs, a dominant y-polarization state can be encoded as $|+1\rangle$ and a dominant x-polarization state can be encoded as $|-1\rangle$.

In such a system of injection-locked lasers, the ground state search of the Hamiltonian is performed through the mechanism of mode competition resulting from cross-gain saturation when a system of lasers is mutually injection-locked. When photons of different polarizations enter a VCSEL's cavity through injection-locking, provided that there is sufficient spectral overlap with the gain and cavity, the laser's spectrum can be modified resulting in a peak at the injected frequency. The various polarized modes then compete for the highest gain. Eventually, a particular mode in the VCSEL will consume most of the available gain and suppress the gain available to the other mode. This can have the effect of switching the lasing mode in the laser. The authors from a paper describing an Ising solver using an injection-locked multicore fiber laser attribute the ability of the system to find minima as one that is observed, rather than something mathematically rigorous.[4] However, some work has been done mapping polarization-resolved laser rate equations in the multicore fiber laser example to the Lagrangian optimization problem.[24]

A simplified picture of this scheme is shown in Fig. 1, with a configuration similar to that of Utsunomiya et al.[1] but with linear polarizations instead of circular (to match the natural polarization bistability found in VCSELs). The attenuator and the half-wave plate (HWP) in the optical path between the VCSELs allow for the tuning of the magnitude and polarity of the Ising interaction term, J_{ij}. The absence of the HWP implements a negative interaction term J_{ij}, whereas the presence of an HWP implements a positive interaction term J_{ij}. The Zeeman term in the Ising model is implemented with a master laser, which injection locks the VCSELs in a unidirectional manner. The isolator between the master laser and the slave VCSELs prevents the VCSELs from interfering with the master laser's emission. The magnitude and the polarity of the Zeeman term implemented in this scheme is controlled with an attenuator and an HWP at 45 deg. By adjusting the interactions between the VCSELs, one can program any arbitrary Ising problem to be solved. While the scheme pictured in Fig. 1 may seem overly complicated, we believe it is possible to achieve multiple interactions in parallel (with a large array of VCSELs) with an appropriate sequence of linear optical elements programming the interaction terms, and individual interaction
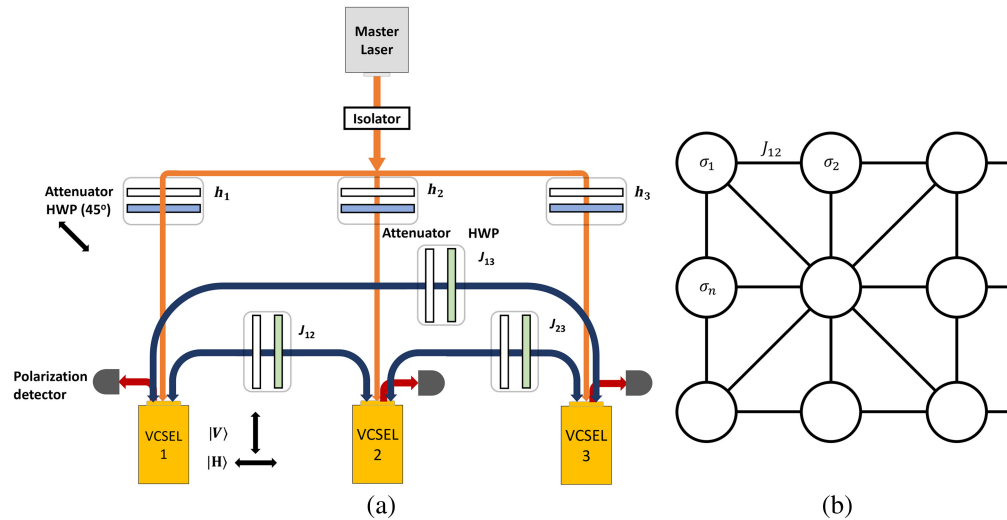
Fig. 1 (a) Proposed VCSEL-based injection-locked Ising solver, based on a similar circular polarization-based laser injection locking scheme by Utsunomiya et al.[1] Such a scheme solves the Ising problem shown in (b).

paths like those pictured would then not be needed, although this would be a subject for further study.

This paper seeks to answer two key questions necessary for the development of a VCSEL-based injection-locked Ising computer. It is not known if such a scheme using the linear polarization directions of VCSELs is able to adequately solve Ising problems. Previous work on injection-locked laser-based Ising solvers focuses on the use of circular polarization states to encode Ising spins,[1] which does not reflect a real VCSEL's behavior of favoring linear polarization states.[25] In addition to this, it is not presently clear if a master laser is required to initialize the VCSELs into a diagonally polarized state. Such a state represents a halfway state between the final horizontal and vertical polarized states required for a solution. The subsequent injection locking from other VCSELs into each other would force this halfway state into either a horizontal or vertical polarization state. This paper answers these questions by using the spin-flip model (SFM), which describes the dynamics of the linear polarization states in VCSELs, to model a system of injection-locked VCSELs capable of solving Ising problems.

2 Theoretical Model

2.1 Introduction to the Spin-Flip Model

The SFM provides a theoretical framework for modeling the polarization bistability of the x- and y-polarized modes in VCSELs. It considers the coupling of the vector field to the saturable dispersion in birefringent materials, which is quantified in the parameter α, also known as the linewidth enhancement factor. The value of α reflects the degree to which the modulation of the refractive index impacts the cavity resonance frequency and is an important factor in determining the dynamic behavior of VCSELs. The SFM models the spin relaxations between the transitions that give rise to right and left circularly polarized light in a VCSEL, which is represented by the parameter γ_s. This parameter accounts for the reduction in the differences in the sub-level population that arise from the presence of different numbers of electrons in spin-up and spin-down states. Instead of modeling the circularly polarized fields arising from the transitions in the VCSEL, a simple change of basis can be introduced to model the x- and y-polarized fields while maintaining the aforementioned parameters. These x- and y-modes in the VCSEL have a frequency splitting modeled by the linear phase anisotropy parameter, γ_p. These two modes may also have different gain-to-loss ratios, modeled by the gain anisotropy parameter, γ_a.

The SFM equations for the electric field in a VCSEL as in Refs. 26 and 27 model the electric field in a VCSEL, which is presented as

$$e_x = E_x e^{i\omega_x t + i\phi_x} = E_x e^{i(\alpha\gamma_a - \gamma_p)t + i\phi_x}, \tag{2}$$

$$e_y = E_y e^{i\omega_y t + i\phi_y} = E_y e^{i(\gamma_p - \alpha\gamma_a)t + i\phi_y}, \tag{3}$$

consider the coupling of the vector field to the saturable dispersion in birefringent materials, which is well documented in the literature.[28] In Eqs. (2) and (3), $E_{x,i}$ ($E_{y,i}$) represents the amplitude of the x- (y-) polarized photon field of VCSEL i, whereas $\phi_{x,i}$ ($\phi_{y,i}$) represents the phase of the x- (y-) polarized mode. ω_x and ω_y are the angular frequencies of the x- and y-polarized modes, respectively. ϕ_x and ϕ_y are the phases of the x- and y-polarized modes, respectively.

The electric field of the injected light into the cavity of a VCSEL can be written in its x- and y-components, which are given as

$$e_{\mathrm{inj},x} = E_{\mathrm{inj},x} e^{i\delta_x}, \tag{4}$$

$$e_{\mathrm{inj},y} = E_{\mathrm{inj},y} e^{i\delta_y}. \tag{5}$$

The phase $\delta_y = 0$ can be set and $\delta_x = \delta$ can be defined. This models the relative phase between the x- and y-polarized modes, allowing an injected signal of any arbitrary polarization to be set by changing the value of δ, which represents the phase between the modes, and angle of linear polarization through

$$E_{\mathrm{inj},x} = E_{\mathrm{inj},y} \tan \theta_p. \tag{6}$$

Using these equations, the entire SFM for a single VCSEL under injection locking from a master laser is given as[26,27]

$$\frac{dE_x}{dt} = \kappa[(N-1)E_x - mE_y(\sin \Delta\phi + \alpha \cos \Delta\phi)]$$
$$- \gamma_a E_x + K_{\mathrm{inj}} E_{\mathrm{inj},x} \cos \Delta x + \sqrt{\beta_{\mathrm{sp}}(N+m)}\xi(t), \tag{7}$$

$$\frac{dE_y}{dt} = \kappa[(N-1)E_y + mE_x(\alpha \cos \Delta\phi - \sin \Delta\phi)]$$
$$+ \gamma_a E_y + K_{\mathrm{inj}} E_{\mathrm{inj},y} \cos \Delta y + \sqrt{\beta_{\mathrm{sp}}(N-m)}\xi(t), \tag{8}$$

$$\frac{d\phi_x}{dt} = \kappa\left[\alpha(N-1) + m\frac{E_y}{E_x}(\cos \Delta\phi - \alpha \sin \Delta\phi)\right] - \Delta\omega - \alpha\gamma_a + K_{\mathrm{inj}}\frac{E_{\mathrm{inj},x}}{E_x} \sin \Delta x, \tag{9}$$

$$\frac{d\phi_y}{dt} = \kappa\left[\alpha(N-1) - m\frac{E_x}{E_y}(\alpha \sin \Delta\phi + \cos \Delta\phi)\right] - \Delta\omega + \alpha\gamma_a + K_{\mathrm{inj}}\frac{E_{\mathrm{inj},y}}{E_y} \sin \Delta y, \tag{10}$$

$$\frac{dN}{dt} = -\gamma[N(1 + E_x^2 + E_y^2) - \eta - 2mE_y E_x \sin \Delta\phi], \tag{11}$$

$$\frac{dm}{dt} = -\gamma_s m - \gamma[m(E_x^2 + E_y^2)] + 2\gamma N E_y E_x \sin \Delta\phi. \tag{12}$$

The parameter K_{inj} represents the injection coupling coefficient, which characterizes the strength of the injection locking effect. κ is the photon decay rate, N is the population difference between the conduction and valence bands, m is the normalized difference in allowed transitions between the two magnetic sublevels present in VCSELs, and η is the normalized pumping rate. The noise terms associated with spontaneous emission in the laser cavity are encapsulated by the parameter β_{sp}, which represents the spontaneous emission factor. The term ξ represents the Gaussian noise with a mean of 0 and a standard deviation of 1. The other simplified terms in the equations are given by $\Delta\phi = 2(\gamma_p - \alpha\gamma_a)t + \phi_y - \phi_x$, $\Delta x = \omega_y t - \phi_x + \delta$, and $\Delta y = \omega_x t - \phi_y$.

2.2 Extending the Spin-Flip Model for Mutual Injection-Locking

We now depart from established theory to model a system of mutually injection-locked VCSELs. By assigning an index i to each variable in the system of coupled differential equations,

additional terms, $e_{x,j}$ and $e_{y,j}$, as defined in Eqs. (2) and (3), can be incorporated in a manner similar to the equations in Refs. 26 and 27. The terms $e_{x,j}$ and $e_{y,j}$ represent the light from VCSEL j that is introduced into VCSEL i, where $j \neq i$. The following set of equations is obtained:

$$\frac{dE_{x,i}}{dt} = \kappa[(N_i - 1)E_{x,i} - m_i E_{y,i}(\sin \Delta\phi_i + \alpha \cos \Delta\phi_i)]$$
$$- \gamma_a E_{x,i} + K_{\text{inj}} E_{\text{inj},x} \cos \Delta x_i + \sqrt{\beta_{\text{sp}}(N_i + m_i)}\xi(t)$$
$$+ K_{\text{inj}} E_{x,j} \cos(\phi_{x,j} - \phi_{x,i}), \tag{13}$$

$$\frac{dE_{y,i}}{dt} = \kappa[(N_i - 1)E_{y,i} + m_i E_{x,i}(\alpha \cos \Delta\phi_i - \sin \Delta\phi_i)]$$
$$+ \gamma_a E_{y,i} + K_{\text{inj}} E_{\text{inj},y} \cos \Delta y_i + \sqrt{\beta_{\text{sp}}(N_i - m_i)}\xi(t)$$
$$+ K_{\text{inj}} E_{y,j} \cos(\phi_{y,j} - \phi_{y,i}), \tag{14}$$

$$\frac{d\phi_{x,i}}{dt} = \kappa\left[\alpha(N_i - 1) + m_i \frac{E_{y,i}}{E_{x,i}}(\cos \Delta\phi_i - \alpha \sin \Delta\phi_i)\right]$$
$$- \Delta\omega - \alpha\gamma_a + K_{\text{inj}} \frac{E_{\text{inj},x}}{E_{x,i}} \sin \Delta x_i$$
$$+ K_{\text{inj}} \frac{E_{x,j}}{E_{x,i}} \sin(\phi_{x,j} - \phi_{x,i}), \tag{15}$$

$$\frac{d\phi_{y,i}}{dt} = \kappa\left[\alpha(N_i - 1) - m_i \frac{E_{x,i}}{E_{y,i}}(\alpha \sin \Delta\phi_i + \cos \Delta\phi_i)\right]$$
$$- \Delta\omega + \alpha\gamma_a + K_{\text{inj}} \frac{E_{\text{inj},y}}{E_{y,i}} \sin \Delta y_i$$
$$+ K_{\text{inj}} \frac{E_{y,j}}{E_{y,i}} \sin(\phi_{y,j} - \phi_{y,i}), \tag{16}$$

$$\frac{dN_i}{dt} = -\gamma[N_i(1 + E_{x,i}^2 + E_{y,i}^2) - \eta - 2m_i E_{y,i} E_{x,i} \sin \Delta\phi_i], \tag{17}$$

$$\frac{dm_i}{dt} = -\gamma_s m_i - \gamma[m_i(E_{x,i}^2 + E_{y,i}^2)] + 2\gamma N_i E_{y,i} E_{x,i} \sin \Delta\phi_i. \tag{18}$$

The contributions of multiple VCSELs coupling to the i'th VCSEL in an M-VCSEL system can be combined. The couplings from other VCSELs ($j \neq i$) into the amplitude of the x-polarized mode (E_x) of the i'th VCSEL are denoted by $\varepsilon_{x,ji}$. These contributions can be further split into two terms: those from the x-polarized modes of other VCSELs ($j \neq i$), and those from the y-polarized modes of other VCSELs ($j \neq i$) where an HWP is placed between the VCSEL interaction paths. In the latter case, the x-polarized mode of VCSEL j couples into the y-polarized mode of VCSEL i, and the y-polarized mode of VCSEL j couples into the x-polarized mode of VCSEL i due to the insertion of an HWP. Similarly, $\varepsilon_{y,ji}$ contains information on the couplings from other VCSELs ($j \neq i$) into the y-polarized mode of VCSEL i. With these definitions, the following equations can be defined:

$$\varepsilon_{x,ji} = \varepsilon_{xx,ji} + \varepsilon_{yx,ji}, \tag{19}$$

$$\varepsilon_{y,ji} = \varepsilon_{yy,ji} + \varepsilon_{xy,ji}. \tag{20}$$

The subscript yx in $\varepsilon_{yx,ji}$ indicates that the y-polarized mode of VCSEL j is coupled into the x-polarized mode of VCSEL i due to the presence of an HWP. Similarly, the subscript xy indicates the reverse process. The interactions from the x-polarized mode in VCSEL j into the x-polarized mode of VCSEL i and the y-polarized mode in VCSEL j into the y-polarized mode of VCSEL i can be represented by a coupling matrix $A = (a_{ji})$. This symmetric matrix represents the strength of coupling between the j'th and i'th sites without the presence of an HWP.

Interactions where an HWP is present are indicated with a zero. Because the light must pass both ways, the strength of coupling must be identical from j to i and vice versa, leading to a symmetric matrix. In addition, the diagonal of the matrix is zero, as the i'th VCSEL site cannot be coupled to itself. Therefore, a_{ji} has the following properties:

$$a_{ji} = a_{ij}, \quad a_{ii} = 0, \quad 0 \leq a_{ji} \leq 1. \tag{21}$$

The interactions from the x-polarized mode to the y-polarized mode and vice versa can be represented by the matrix $A_{\mathrm{HWP}} = (a_{\mathrm{HWP},ji})$, which denotes interactions where an HWP is introduced. Interactions where an HWP is absent are indicated with a zero. This is a symmetric matrix that represents the strength of coupling between VCSEL sites. The properties of $a_{\mathrm{HWP},ji}$ are as follows:

$$a_{\mathrm{HWP},ji} = a_{\mathrm{HWP},ij}, \quad a_{\mathrm{HWP},ii} = 0, \quad 0 \leq a_{\mathrm{HWP},ji} \leq 1. \tag{22}$$

Because the elements in A represent the negative Ising interactions and the elements in A_{HWP} represent the positive Ising interactions, the Ising interaction matrix can then be written as

$$J = -A + A_{\mathrm{HWP}}. \tag{23}$$

Following the same procedure used in adding the terms introduced by a master laser, $\varepsilon_{x,ji}$ and $\varepsilon_{y,ji}$ can be expressed as

$$\varepsilon_{x,ji} = \varepsilon_{xx,ji} + \varepsilon_{yx,ji}$$
$$= K_{\mathrm{inj}} \sum_{j \neq i}^{M} [a_{ji} E_{x,j} \cos(\phi_{x,j} - \phi_{x,i}) + a_{\mathrm{HWP},ji} E_{y,j} \cos(\omega_y - \omega_x + \phi_{y,j} - \phi_{x,i})], \tag{24}$$

$$\varepsilon_{y,ji} = \varepsilon_{yy,ji} + \varepsilon_{xy,ji}$$
$$= K_{\mathrm{inj}} \sum_{j \neq i}^{M} [a_{ji} E_{y,j} \cos(\phi_{y,j} - \phi_{y,i}) + a_{\mathrm{HWP},ji} E_{x,j} \cos(\omega_x - \omega_y + \phi_{x,j} - \phi_{y,i})]. \tag{25}$$

The contributions of injection locking to the phase terms, $\phi_{x,i}$ and $\phi_{y,i}$, can be written by replacing the cosine terms in Eqs. (24) and (25) with sine terms, and dividing the polarization-resolved phase term by its polarization-resolved amplitude. This yields the following expressions:

$$\Phi_{x,ji} = \Phi_{xx,ji} + \Phi_{yx,ji}$$
$$= \frac{1}{E_{x,i}} K_{\mathrm{inj}} \sum_{j \neq i}^{M} [a_{ji} E_{x,j} \sin(\phi_{x,j} - \phi_{x,i}) + a_{\mathrm{HWP},ji} E_{y,j} \sin(\omega_y - \omega_x + \phi_{y,j} - \phi_{x,i})], \tag{26}$$

$$\Phi_{y,ji} = \varepsilon_{yy,ji} + \varepsilon_{xy,ji}$$
$$= \frac{1}{E_{y,i}} K_{\mathrm{inj}} \sum_{j \neq i}^{M} [a_{ji} E_{y,j} \sin(\phi_{y,j} - \phi_{y,i}) + a_{\mathrm{HWP},ji} E_{x,j} \sin(\omega_x - \omega_y + \phi_{x,j} - \phi_{y,i})]. \tag{27}$$

These terms make up the coupling from $j \neq i$ VCSELs into the i'th VCSEL's amplitudes and phase. Using Eqs. (24)–(27), the coupled VCSEL system can finally be written as

$$\frac{dE_{x,i}}{dt} = \kappa[(N_i - 1)E_{x,i} - m_i E_{y,i}(\sin \Delta\phi_i + \alpha \cos \Delta\phi_i)]$$
$$- \gamma_a E_{x,i} + K_{\mathrm{inj}} E_{\mathrm{inj},x} \cos \Delta x_i + \sqrt{\beta_{\mathrm{sp}}(N_i + m_i)}\xi(t) + \varepsilon_{x,ji}, \tag{28}$$

$$\frac{dE_{y,i}}{dt} = \kappa[(N_i - 1)E_{y,i} + m_i E_{x,i}(\alpha \cos \Delta\phi_i - \sin \Delta\phi_i)]$$
$$+ \gamma_a E_{y,i} + K_{\mathrm{inj}} E_{\mathrm{inj},y} \cos \Delta y_i + \sqrt{\beta_{\mathrm{sp}}(N_i - m_i)}\xi(t) + \varepsilon_{y,ji}, \tag{29}$$

$$\frac{d\phi_{x,i}}{dt} = \kappa\left[\alpha(N_i - 1) + m_i\frac{E_{y,i}}{E_{x,i}}(\cos\,\Delta\phi_i - \alpha\,\sin\,\Delta\phi_i)\right]$$
$$- \Delta\omega - \alpha\gamma_a + K_{inj}\frac{E_{inj,x}}{E_x}\,\sin\,\Delta x_i + \Phi_{x,ji}, \tag{30}$$

$$\frac{d\phi_{y,i}}{dt} = \kappa\left[\alpha(N_i - 1) - m_i\frac{E_{x,i}}{E_{y,i}}(\alpha\,\sin\,\Delta\phi_i + \cos\,\Delta\phi_i)\right]$$
$$- \Delta\omega + \alpha\gamma_a + K_{inj}\frac{E_{inj,y}}{E_{y,i}}\,\sin\,\Delta y_i + \Phi_{y,ji}, \tag{31}$$

$$\frac{dN_i}{dt} = -\gamma[N_i(1 + E_{x,i}^2 + E_{y,i}^2) - \eta - 2m_iE_{y,i}E_{x,i}\,\sin\,\Delta\phi_i], \tag{32}$$

$$\frac{dm_i}{dt} = -\gamma_s m_i - \gamma[m_i(E_{x,i}^2 + E_{y,i}^2)] + 2\gamma N_iE_{y,i}E_{x,i}\,\sin\,\Delta\phi_i. \tag{33}$$

These equations will be used to simulate an injection-locked VCSEL-based Ising computer.

3 Simulated Injection-Locked VCSEL-Based Ising Computer

This section details the methods and the results in the simulation of a system of injection-locked VCSELs. First, the injection locking between a single master and slave will be explored. The injection-locking between the master and slave initializes the VCSEL into an unstable diagonally polarized state. After which, a selection of 2-, 3-, and 4- bit Ising problems will be simulated using the extension of the SFM with Eqs. (28)–(33). The results of the simulations will also be discussed, and the performance of the Ising solver with and without the master laser will be compared.

3.1 Methods

3.1.1 Parameters in the model

The parameters were used in the model, taken from Ref. 26, are found in Table 1. These parameters are from a 1550 nm VCSEL, with a number of parameters calculated from the optical characteristics of the VCSEL by the authors of Ref. 26. The 1550 nm VCSEL supports both the x- and y-polarized modes with a wavelength difference of 0.5 nm between them. The VCSEL has a threshold current of 2.05 mA.

Table 1 Parameter values for the simulation of injection locking dynamics.

Parameter	Value
γ	0.67 ns^{-1}
γ_a	0.02 ns^{-1}
γ_p	192 rad/ns
γ_s	1000 ns^{-1}
κ	125 ns^{-1}
η	3.4
K_{inj}	35.5 ns^{-1}
α	3
β_{sp}	10^{-5}

3.1.2 *Computational methods*

For simple injection locking between a slave laser and master laser, Runge-Kutta 45 (RK45) is sufficient. However, for more complex interactions between multiple mutually injection-locked VCSELs, Ito's lemma was employed to better handle the equations' stochastic nature. Ito's lemma is given as

$$dS_t = F dt + G dW. \tag{34}$$

The equation for Ito's lemma includes a Wiener process W, and deterministic functions F and G. The solution S_t for S at time t is also included. In our model, G contains the terms associated with the Gaussian noise ξ. The combination of Ito's lemma and Euler–Maruyama's algorithm is employed for the coupled-VCSEL Ising computer simulations.

3.1.3 *Time and parameter steps for injection locking dynamics simulations*

Using a small time step in the simulation allows for more accurate modeling of the laser dynamics and better resolution in the resulting data. The shortest transitions in lasers, known as relaxation oscillations, occur on the order of nanoseconds, so using a time step of $t = 1$ ps ensures that the simulation captures these fast dynamics.

Similarly, a wavelength step of 0.01 nm is used in the frequency sweeps to ensure that the simulation captures the subtle changes in laser behavior as the detuning and injection power are varied.

3.2 Master Laser Injection Locking Dynamics

A key question in the design of an injection-locked VCSEL Ising solver is the necessity of a master laser for the system. The master laser could be used to initialize the VCSEL polarizations into an unstable diagonal state, which facilitates polarization switching to either the y- or x-directions. Equations (7)–(12) were used to simulate the injection locking of a single VCSEL using a master laser with diagonal polarization ($E_{\text{inj},x} = E_{\text{inj},y}$ and $\delta = 0$). A frequency detuning range of −60 to 60 GHz was simulated for various injection power levels, as set by $E_{\text{inj},x} = E_{\text{inj},y}$. The master laser's injected signal was introduced at time $t = 25$ ns, and each data point was simulated 10 times to account for the noise terms in the equations. To measure how closely the slave laser aligns with the injected signal's polarization, the angle θ is defined as follows:

$$\theta = \arctan\left(\frac{E_{y,\text{avg}}}{E_{x,\text{avg}}}\right), \tag{35}$$

where $E_{y,\text{avg}}$ and $E_{x,\text{avg}}$ are the average y- and x-polarized field amplitudes of the slave VCSEL's emission in the last 5 ns of the simulation, and θ is in degrees. Figure 2 shows the plot
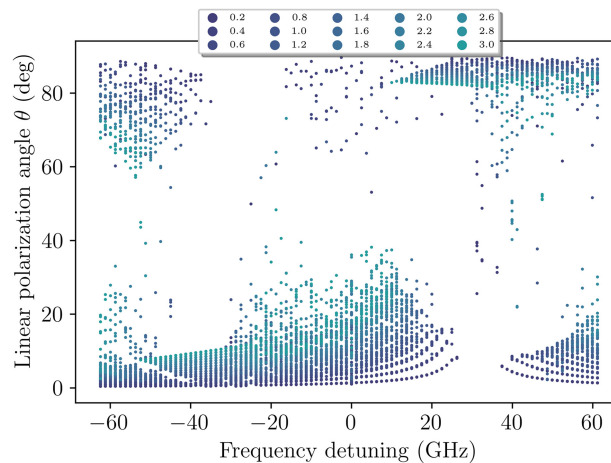
Fig. 2 Linear polarization direction (θ) against injection frequency detuning for various injection field amplitudes when the master laser is diagonally polarized.
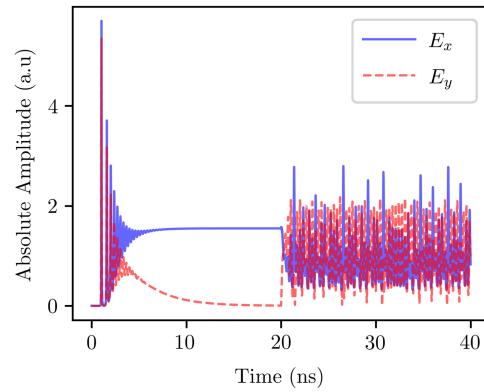
Fig. 3 Injection locking of a VCSEL by a master laser at $E_{\text{inj},x} = E_{\text{inj},y} = 0.2$ and a frequency detuning of 31.14 GHz.

of the angle θ against injection frequency detuning for various injection field amplitudes $E_{\text{inj},x} = E_{\text{inj},y}$.

The results in Fig. 2 indicate that the allowable range of frequencies that affect the slave VCSEL's polarization state increases with increasing injected field amplitude. As the injection amplitude is increased, the master laser is better able to affect the polarization angle of the slave VCSEL. The frequency detuning range at which the master laser affects the slave laser also increases with increasing injection amplitude. The asymmetric locking range results from the change in index of refraction of the cavity when the VCSEL is injection-locked.[29] When the frequency detuning is too great, the threshold gain of the laser is too high and the VCSEL returns to the preferred unlocked operation.[19] Figure 2 demonstrates some diagonal symmetry; however, the VCSEL prefers the free-running polarization angle of 0 deg, as opposed to 90 deg. This leads to a greater cluster of points at the bottom of the figure, as opposed to the top.

The injection locking with a frequency detuning in the region between 20 and 40 GHz leaves the slave VCSEL in an unstable state, which is evidenced by the data points at injection levels of $E_{\text{inj},x} = E_{\text{inj},y} = 0.2$ closest to $\theta = 45$ deg. The instability is further highlighted by the data points that flip to $\theta = 90$ deg, indicating that the E_y polarization becomes dominant. At higher injection field amplitudes, the linear polarization orientations in the region 20 to 40 GHz are more likely to flip than to take on a direction near $\theta = 45$ deg.

Therefore, low injection power, along with a frequency detuning of around 30 GHz, favors the initialization of the slave VCSEL into an unstable, diagonally polarized state.

Figure 3 shows a plot of E_x and E_y from a VCSEL at an injection field amplitude of $E_{\text{inj},x} = E_{\text{inj},y} = 0.2$ and a frequency detuning of 31.14 GHz.

The simulation in Fig. 3 indicates a linear polarization angle of $\theta = 48.0$ deg emitted from the injection-locked VCSEL. This frequency detuning of 31.14 GHz will serve as a useful reference point in subsequent simulations, as it can be used to initialize the VCSEL system into an unstable diagonal polarization state.

3.3 Ising Simulations

We now investigate Ising systems of mutual injection-locked VCSELs. To illustrate, consider a 2-bit Ising problem, where two VCSELs, namely VCSEL 1 and VCSEL 2, are directed at each other resulting in bidirectional coupling. As previously mentioned, in the absence of an HWP, this configuration gives rise to the interaction term $J_{12} = J_{21} = -1$. Following the equation for the Ising model in Eq. (1), the solution to this problem entails both VCSELs having either $|+1\rangle$ or $|-1\rangle$ states, which can be expressed as either $(+1, +1)$ or $(-1, -1)$ when minimizing the Hamiltonian in Eq. (1). On the other hand, when an HWP is placed between the VCSELs, the interaction term $J_{12} = J_{21} = 1$ is introduced and the solution to this problem becomes $(+1, -1)$ or $(-1, +1)$. The ability of the VCSEL-system to solve such Ising problems is evaluated through a selection of 2-, 3-, and 4-bit Ising problems whose Hamiltonians are given as
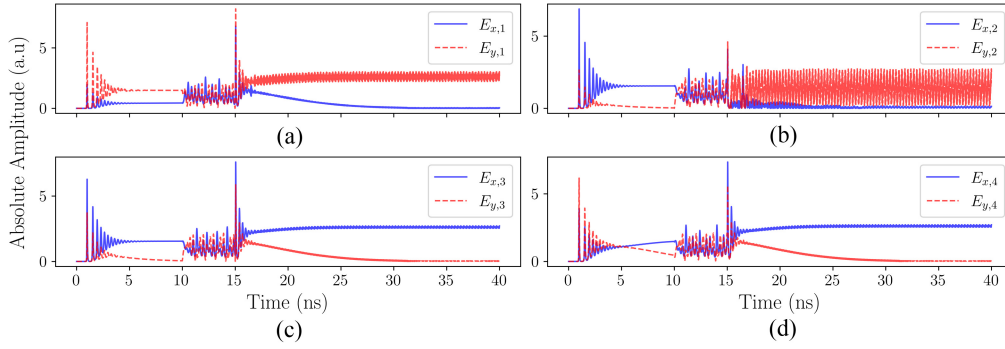
Fig. 4 Dynamics of the first 4-bit injection-locked VCSEL Ising system with master laser activated at 10 ns and mutual VCSEL couplings activated at 15 ns. The VCSELs are labeled (a), (b), (c), and (d).

$$J^2 = \begin{bmatrix} 0 & -1 \\ -1 & 0 \end{bmatrix}, \quad J^3 = \begin{bmatrix} 0 & -1 & 0 \\ -1 & 0 & 1 \\ 0 & 1 & 0 \end{bmatrix} \quad J^4 = \begin{bmatrix} 0 & -1 & 1 & 1 \\ -1 & 0 & 0 & 0 \\ 1 & 0 & 0 & -1 \\ 1 & 0 & -1 & 0 \end{bmatrix}, \tag{36}$$

where the superscript denotes the system size. Equations (28)–(33) were used to model this system. In all simulations, the master laser is activated at 10 ns and the mutual couplings between VCSELs are activated at 15 ns. If no master laser is used, the VCSEL couplings are still activated at 15 ns. For each system, 5000 iterations were performed. The dominant polarization state is determined by calculating the average values of the absolute values of E_x and E_y for the last 5 ns of the simulation.

A particular instance of the VCSEL system dynamics when solving the 4-bit Ising problem in Eq. (36) is shown in Fig. 4. The solution provided in Fig. 4 is $(+1, +1, -1, -1)$.

The same Ising system is then solved without a master laser present. Figure 5 shows the dynamics of one particular iteration, the solution of which is $(-1, -1, 1, 1)$. Both solutions shown in Figs. 4 and 5 are valid solutions to the Ising problem being solved.

The overall performance of the Ising solvers can be evaluated by calculating the probability of the solver being able to pick out the right solution that minimizes the Hamiltonian. Each Ising system has a total of 2^M possible outcomes. A purely random Ising solver would pick out each of these solutions with equal probability or $1/2^M$. To assess the proposed Ising solver's ability to find the correct solution out of the possible 2^M solutions, a right-tailed p-test is conducted on the data for each simulation. The p-value (correct) is calculated from the probability $\mathbb{P}(\text{Correct})$, which represents the probability of the solver finding the correct solution out of the 5000 runs simulated.

Another metric of interest is the ability of the solver to find alternate solutions. Each problem presented in Eq. (36) has two solutions. An unbiased Ising solver should provide each of these correct solutions with equal frequency. A two-tailed p-test is conducted to test if the correct
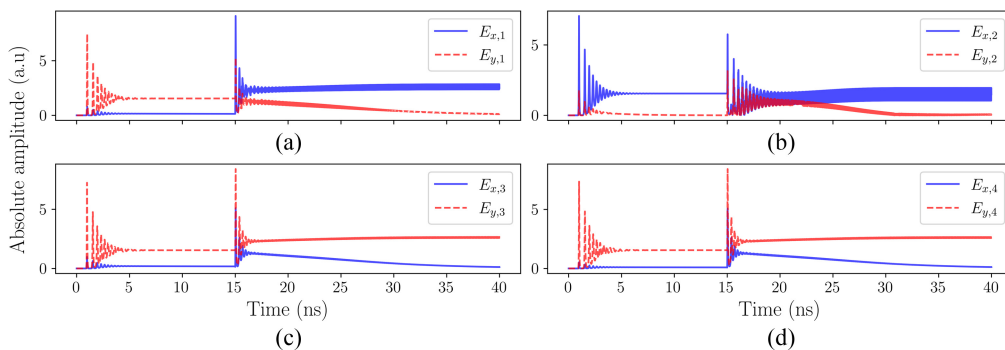
Fig. 5 Dynamics of the first 4-bit injection-locked VCSEL Ising system without a master laser. Mutual VCSEL couplings are activated at 15 ns. The VCSELs are labeled (a), (b), (c), and (d).

Table 2 Performance of simulated Ising solvers.

System size	Master	IP (correct)	p-value (correct)	IP (alternate)	p-value (alternate)
2	✓	1	0	0.497	0.365
	—	1	0	0.494	0.365
3	✓	0.843	0	0.452	6.61×10^{-10}
	—	0.998	0	0.324	2.80×10^{-136}
4	✓	0.581	0	0	0
	—	0.317	0	0.011	0

solutions found by the system appear with a probability of 0.5. This probability is denoted as IP(Alternate), and in an ideal Ising solver, it should be IP(Alternate) = 0.5.

The p-values obtained from the analyses provide strong evidence that the proposed Ising solver is capable of finding the correct solution to the Ising problem with a probability better than random chance. However, it is worth noting that the solver's performance deteriorates as the system size increases. Furthermore, the probability of one of the two correct solutions being chosen (IP (Alternate)) decreases away from the ideal value of 0.5 as the system size increases, except for the case of system size 2. This implies that the solver's ability to find multiple correct solutions with equal probability decreases as the system size increases (Table 2).

In the 2- and 3-bit cases, the master laser does not appear to play a significant role in the Ising solver's ability to find the correct solution. However, an interesting phenomenon is observed in the 4-bit case: when solved with a master laser, the solution $(-1, -1, +1, +1)$ never occurs, whereas the same solution occurs significantly more often (1568 out of 5000 trials) in the absence of the master laser. This suggests that the master laser may affect the relative stability of the x- and y-polarization modes, thereby favoring certain solutions. However, this may not necessitate the removal of the master laser, as it may be able to implement more complex Ising problems through the Zeeman term h_i.

Though the Ising solver proposed in this paper does not always achieve the global minimum, it achieves at least the second lowest global minimum all the time, and although the number of bits simulated is small, we can at least be sure that the system will favor lower energy states. Despite the inability of the system to find the global minimum with every trial, results from any Ising solver can still be useful as long as they provide a solution sufficiently close enough to a global minimum.

3.4 Influence of SFM Model Parameters

Certain parameters in the SFM give preference to either the y- or x-polarized modes in the VCSEL. In an ideal Ising solver, the preference for both of these modes should be equal. The γ_p term models the phase anisotropy experienced by the y- and x-polarized modes in the VCSEL, introduced by the crystal birefringence. The parameter γ_a models the amplitude anisotropy, which provides the y- and x-polarized modes with different gain-to-loss ratios. Other parameters that influence the VCSEL's preferred polarization mode, and the stability of these modes, are the normalized injection current, η and the ratio γ_p/γ.[28]

The effect of these parameters can be seen when a free-running VCSEL is simulated. In this simulation, the VCSEL is turned on without any external disturbance. The final polarization state of the VCSEL can then be measured. Using the parameters in Table 1, the free-running VCSEL is simulated 1000 times. Keeping with the convention of the y-polarized mode having the $|+1\rangle$ state and the x-polarized mode having the $|-1\rangle$ state, the simulation is found to favor the $|+1\rangle$ state 45 times, whereas the $|-1\rangle$ state is favored 955 times. This is not ideal, as it means that the VCSEL design parameters heavily favor certain polarization modes over others, thereby resulting in particular Ising solutions to be favored over others as well.

By performing a naive sweep of the variable γ_a, the change in the probability of the VCSEL obtaining a final $|-1\rangle$ state can be observed. The data from this naive sweep are shown in Fig. 6.
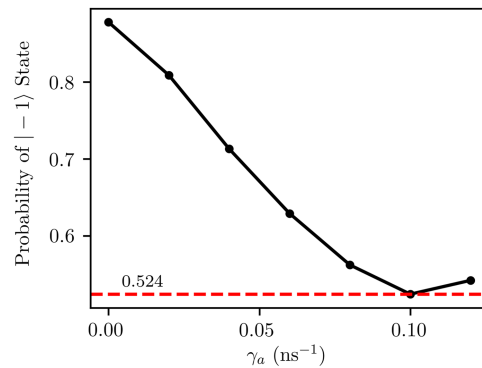
Fig. 6 Probability of free-running VCSEL having a $|-1\rangle$ final state when the parameter γ_a is varied.

It is clear that the parameter γ_a plays a significant role in making the VCSEL Ising solver unbiased. The naive sweep shows a minimum where the probability of the x- and y-polarized mode occurring is almost 0.5. Our (assumed realistic) value for γ_a does not favor the x- and y-polarized modes equally. This leads to particular Ising solutions being favored over others.

The second parameter that influences the probability of the x- and y-polarized states occurring is γ_p/γ. The probability of the $|-1\rangle$ state occurring—almost 0.9—when $\gamma_a = 0$ as shown in Fig. 6 is an unexpected result, as a lack of difference in gain-to-loss ratios between the two modes should yield a near 50/50 chance of each mode occurring. This can be remedied by changing the value of η and γ_p/γ to one that ensures the stability of both the x- and y-modes.[28] Setting $\eta = 1.2$ and $\gamma_p/\gamma = 9$ with $\gamma = 1$ ns^{-1} resulted in the $|-1\rangle$ state occurring with a probability of 0.499. Keeping this ratio of $\gamma_p/\gamma = 9$ and $\eta = 1.2$ but setting $\gamma_a = 0.02$ ns^{-1}, as was originally used for the Ising simulations, and $\gamma_a = 0.1$ ns^{-1}, as was previously identified as the value at which the probability of the x- and y-polarized modes occur nearly half the time, resulted in a probability of 0.32 and 0.019 that the $|-1\rangle$ state occurs, respectively. Furthermore, changing these parameters for the Ising problem simulations resulted in variations in probability of the system finding the correct solution to the Ising problem.

It is clear that both the parameters γ_a and γ_p/γ influence the probability of the $|-1\rangle$ state occurring, although the relationship the parameters γ_a and γ_p/γ have on the probability of the $|-1\rangle$ state occurring is unclear at the moment. By setting both parameters to one that allows both the x- and y-polarized mode to appear with a probability in a free-running VCSEL, it is likely that an ideal Ising solver can be constructed. There may exist an ideal set of parameters by which the injection-locked VCSEL system can achieve the correct solution with better success. In a realistic Ising machine based on the scheme described, the gain anisotropy and the ratio γ_p/γ could potentially be calibrated away through engineered current injection anisotropy or clever cavity design.

4 Conclusion

The VCSEL-based Ising solver modeled using the SFM is able to solve the selected Ising problems significantly better than chance. A potential concern that would affect any Ising solver constructed based on the scheme described would be the preference of the system to prefer certain Ising configurations over others of nominal equal energy, as a result of the parameter γ_p/γ and the built-in polarization gain anisotropy in VCSELs, which we modeled in parameter γ_a. Future work could encompass modeling and fabricating VCSELs with equal gain-to-loss ratios between the x- and y-polarized modes, such as through a cruciform cavity geometry.[21] This would allow for each VCSEL to function as an unbiased Ising spin site. Another area relevant for this platform of computing would be the investigation of a linear optical system, which would provide the required Ising interactions for an entire VCSEL array simultaneously, whereby any arbitrary Ising problem could potentially be solved.

Disclosures

Code and Data Availability

Data are available from the authors upon request.

Acknowledgments

References

1. S. Utsunomiya, K. Takata, and Y. Yamamoto, "Mapping of Ising models onto injection-locked laser systems," *Opt. Express* **19**(19), 18091–18108 (2011).
2. S. Utsunomiya et al., "Binary phase oscillation of two mutually coupled semiconductor lasers," *Opt. Express* **23**, 6029 (2015).
3. M. Calvanese Strinati, D. Pierangeli, and C. Conti, "All-optical scalable spatial coherent Ising machine," *Phys. Rev. Appl.* **16**, 54022 (2021).
4. M. Babaeian et al., "A single shot coherent Ising machine based on a network of injection-locked multicore fiber lasers," *Nat. Commun.* **10**(1), 3516 (2019).
5. Y. Okawachi et al., "Demonstration of chip-based coupled degenerate optical parametric oscillators for realizing a nanophotonic spin-glass," *Nat. Commun.* **11**, 4119 (2020).
6. M. Prabhu et al., "Accelerating recurrent Ising machines in photonic integrated circuits," *Optica* **7**, 551 (2020).
7. D. Pierangeli, G. Marcucci, and C. Conti, "Adiabatic evolution on a spatial-photonic Ising machine," *Optica* **7**, 1535 (2020).
8. J. Ouyang et al., "An on-demand photonic Ising machine with simplified hamiltonian calculation by phase-encoding and intensity detection," http://arxiv.org/abs/2207.05072 (accessed 21 December 2023).
9. J. Huang, Y. Fang, and Z. Ruan, "Antiferromagnetic spatial photonic Ising machine through optoelectronic correlation computing," *Commun. Phys.* **4**, 242 (2021).
10. A. Marandi et al., "Network of time-multiplexed optical parametric oscillators as a coherent Ising machine," *Nat. Photonics* **8**, 937–942 (2014).
11. T. Inagaki et al., "A coherent Ising machine for 2000-node optimization problems," *Science* **354**, 603–606 (2016).
12. P. L. McMahon et al., "A fully programmable 100-spin coherent Ising machine with all-to-all connections," *Science* **354**, 614–617 (2016).
13. H. Takesue and T. Inagaki, "10 GHz clock time-multiplexed degenerate optical parametric oscillators for a photonic Ising spin network," *Opt. Lett.* **41**, 4273 (2016).
14. Z. Wang et al., "Coherent Ising machine based on degenerate optical parametric oscillators," *Phys. Rev. A* **88**, 063853 (2013).
15. F. Böhm, G. Verschaffelt, and G. Van der Sande, "A poor man's coherent Ising machine based on opto-electronic feedback systems for solving optimization problems," *Nat. Commun.* **10**(1), 3538 (2019).
16. D. Pierangeli, G. Marcucci, and C. Conti, "Large-scale photonic Ising machine by spatial light modulation," *Phys. Rev. Lett.* **122**, 213902 (2019).
17. S. Kumar, H. Zhang, and Y.-P. Huang, "Large-scale Ising emulation with four body interaction and all-to-all connections," *Commun. Phys.* **3**, 108 (2020).
18. Y. Fang, J. Huang, and Z. Ruan, "Experimental observation of phase transitions in spatial photonic Ising machine," *Phys. Rev. Lett.* **127**, 043902 (2021).
19. L. Chrostowski, "Optical injection locking of vertical cavity surface emitting lasers," PhD thesis, UC Berkeley (1998).
20. D. L. Boiko, G. M. Stéphan, and P. Besnard, "Fast polarization switching with memory effect in a vertical cavity surface emitting laser subject to modulated optical injection," *J. Appl. Phys.* **86**, 4096–4099 (1999).
21. K. D. Choquette et al., "Polarization modulation of cruciform vertical-cavity laser diodes," *Appl. Phys. Lett.* **64**, 2767–2769 (1994).
22. S. Bandyopadhyay et al., "VCSEL polarization control by optical injection," *J. Lightwave Technol.* **21**, 2395 (2003).
23. Z. G. Pan et al., "Optical injection induced polarization bistability in vertical-cavity surface-emitting lasers," *Appl. Phys. Lett.* **63**, 2999–3001 (1993).
24. S. K. Vadlamani, T. P. Xiao, and E. Yablonovitch, "Physics successfully implements Lagrange multiplier optimization," *Proc. Natl. Acad. Sci. U. S. A.* **117**, 26639–26650 (2020).

25. A. A. Qader, Y. Hong, and K. A. Shore, "Lasing characteristics of VCSELs subject to circularly polarized optical injection," *J. Lightwave Technol.* **29**, 3804–3809 (2011).
26. R. Al-Seyab et al., "Dynamics of polarized optical injection in 1550-nm VCSELs: theory and experiments," *IEEE J. Sel. Top. Quantum Electron.* **17**, 1242–1249 (2011).
27. R. Al-Seyab et al., "Dynamics of VCSELs subject to optical injection of arbitrary polarization," *IEEE J. Sel. Top. Quantum Electron.* **19**, 1700512 (2013).
28. J. Martin-Regalado et al., "Polarization properties of vertical-cavity surface-emitting lasers," *IEEE J. Quantum Electron.* **33**(5), 765–783 (1997).
29. R. Lang, "Injection locking properties of a semiconductor laser," *IEEE J. Quantum Electron.* **18**(6), 976–983 (1982).

Brandon Loke received his BE degree in engineering science from the National University of Singapore in 2023. He is currently pursuing his MS degree in electrical and electronics engineering at the École Polytechnique Fédérale de Lausanne.

Biographies of the other authors are not available.